

Support structure constrained topology optimization for additive manufacturing[☆]



Amir M. Mirzendehtdel, Krishnan Suresh^{*}

Department of Mechanical Engineering, University of Wisconsin, Madison, WI 53706, USA

ARTICLE INFO

Article history:

Received 22 December 2015

Accepted 24 August 2016

Keywords:

Topology optimization
Additive manufacturing
3D printing
Support structure
Topological sensitivity
Level-set

ABSTRACT

There is significant interest today in integrating additive manufacturing (AM) and topology optimization (TO). However, TO often leads to designs that are not AM friendly. For example, topologically optimized designs may require significant amount of support structures before they can be additively manufactured, resulting in increased fabrication and clean-up costs.

In this paper, we propose a TO methodology that will lead to designs requiring significantly reduced support structures. Towards this end, the concept of ‘support structure topological sensitivity’ is introduced. This is combined with performance sensitivity to result in a TO framework that maximizes performance, subject to support structure constraints. The robustness and efficiency of the proposed method is demonstrated through numerical experiments, and validated through fused deposition modeling, a popular AM process.

© 2016 Elsevier Ltd. All rights reserved.

1. Introduction

Topology optimization (TO) represents a class of *computational methods* for designing light-weight, high-performance structures [1–3]. After several years of intensive research, it has emerged as a powerful design tool, and is deployed in optimization of aircraft components [4,5], spacecraft modules [6], automobiles components [7], cast components [8], compliant mechanisms [9], etc.

Additive manufacturing (AM), on the other hand, represents a class of *manufacturing processes* for fabricating parts through material addition [10,11]. The growing interest in AM stems from its ability to fabricate highly complex parts with relative ease.

Although TO and AM have flourished independent of each other, there is significant interest today in integrating the two for several reasons [12–16]:

1. Designs stemming from TO are geometrically complex, and therefore hard to manufacture using traditional processes. However, these designs can often be additively manufactured; Fig. 1(a), for example, illustrates a structural design problem that is optimized through TO (Fig. 1(b)), and then fabricated using AM (Fig. 1(c)), with minimal human interference.

2. Since fabrication cost in AM is proportional to the material used, light-weight topology optimized designs are particularly relevant in AM.

In theory, these and other characteristics make TO and AM well suited for each other. However, in practice, topologically optimized designs are often not AM friendly [16,12]. For example, consider the structural problem posed in Fig. 2(a). A topologically optimized design is illustrated in Fig. 2(b); observe the four ‘props’ that improve the structural rigidity but are overhanging (see Section 3.1 for a formal definition of overhanging). These props will require additional support structures to prevent drooping’ (in AM polymer processes) and ‘burning’ (in metal AM processes). Fig. 2(c) illustrates an AM built part with these additional support structures.

Support structures directly add to the build-time and material cost. Material costs can be substantial in AM; for example, the largest percentage cost for metal AM, besides the machine cost that is amortized, is material cost (18%) [17]. Further, support structures can be hard to remove (and sometimes even inaccessible), leading to the *post-fabrication (clean-up) cost*. Post-fabrication costs make-up for about 8% of AM product cost [17].

The objective of this paper is to develop a TO methodology for limiting the support structure volume, thereby leading to designs that are AM friendly. In Section 2, prior research on support structure minimization is reviewed, followed by a review on recent TO advances. In Section 3, the concept of “topological sensitivity for support structures” is introduced, and a methodology to impose

[☆] This paper has been recommended for acceptance by Yong Chen.

^{*} Corresponding author.

E-mail address: suresh@engr.wisc.edu (K. Suresh).

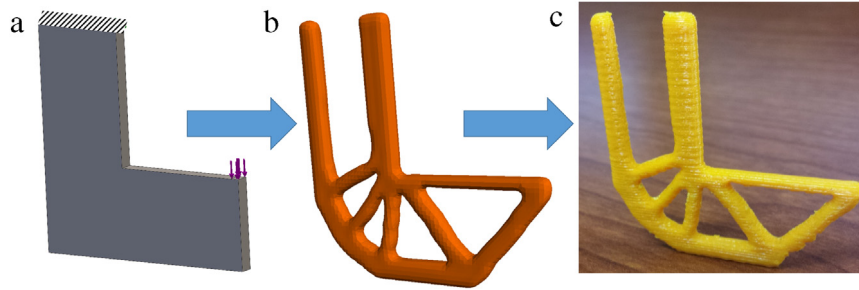


Fig. 1. (a) A structural problem. (b) Topology optimized design. (c) AM fabricated part.

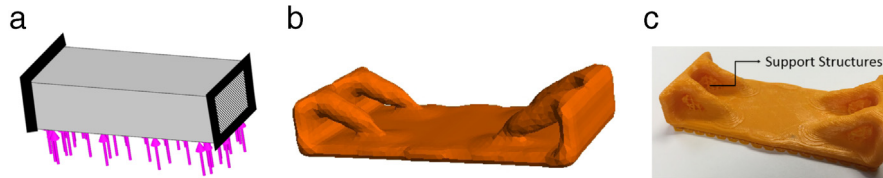


Fig. 2. (a) Structural problem. (b) Optimized topology. (c) Fabricated part with support structures.

support structure constraint during TO is proposed. In Section 4, the efficacy of the proposed methodology is demonstrated through benchmark studies. Section 5 summarizes the contributions of this paper, and discusses future work.

2. Literature review

For reasons stated earlier, support structure minimization is of significant interest within the AM community, and several methods have been proposed. These are classified into the following categories.

Strategy 1: Finding an optimal build direction

AM build-direction can have a significant impact on support structures. Therefore, a popular strategy is to find a build-direction that minimizes support structure volume (and optionally optimizes other AM metrics). For instance, Jibin [18] developed a multi-objective function to find an optimal build direction to minimize volumetric error, support structure, and build time. Along similar lines, Pandey et al. [19] proposed a multi-criteria genetic algorithm to minimize support structure and build time, while improving surface quality. In both instances, weighted averaging was used to solve multi-objective problems. Nezhad et al. [20] proposed tracing the Pareto front to find the optimal part orientation; the Pareto front involved two objective functions, namely support structure and build time. Paul and Anand [21] used a voxel representation (rather than the STL representation) to minimize support structure while satisfying constraints on cylindricity and flatness errors. More recently, Das et al. [22] identified optimal build orientation with respect to tolerance errors and support structure volume by extracting product manufacturing information. Alternate approaches for selecting build-direction include optimizing post-build quality and perception [23], and increased (cross-sectional) mechanical strength [24].

Strategy 2: Generating efficient support structures

While the above methods assume vertical support columns, more efficient support structures have been proposed for a given build-direction. For example, the commercial software Meshmixer™ generates tree-like support structures. While this potentially reduces the support volume, manual modifications are required to ensure printability. Vanek et al. [25] overcame this deficiency by presenting an efficient method for automatically creating tree-like support structures that are printable. Specialized methods have also been proposed for specific AM processes.

For instance, Barnett and Gosselin [26] developed shell and film techniques to create support structures for processes with weak support materials, such as three dimensional foam printers. Dumas et al. [27] exploited scaffolding structures to generate efficient supports for Fused Deposition Modeling (FDM). Considering the stability of the object throughout the build process, the method first identifies support points and then creates horizontal bars between vertical pillars to reduce the support volume. A contour-based support generation scheme was proposed in [28] based on layer-wise analysis. The method first analyzes all of the layers and then generates support anchors using offset and Boolean operations to ensure printability of the part.

Strategy 3: Following design rules for AM

A third strategy is to include support volume constraints during the *manual* design process [29–33]. This is often based on design rules such as [30]: (1) avoid surfaces with large overhang angle, (2) avoid large-size holes (say, larger than 5 mm) [22] perpendicular to the build-direction, (3) avoid trapped surfaces where support structures are hard to remove, and (4) use explicit fillets and chamfers to avoid support structures. Since these rules are feature-based, they are hard to include during TO.

Strategy 4: Optimizing the topology for AM

The final strategy is to include AM constraints within TO. As stated earlier, the advantage of this strategy lies in the (potential) integration of these two technologies.

Imposing manufacturing constraints in TO has been addressed before; a particularly relevant constraint is that of ‘draw-direction constraint’ for casting [34,35], where the TO algorithm was modified so as to avoid ‘inserts’. While this is analogous to the support structure constraint, there are two fundamental differences: (1) support structures are governed by a threshold angle (see Section 3.1) while the threshold angle for draw-direction is essentially zero, and (2) the draw-direction constraint is bidirectional, while the build-direction in AM is unidirectional. Thus, the draw-direction methodology does not apply to AM; novel methods are needed.

Bracket et al. [12] made several recommendations on integrating TO and AM. For example, to minimize support structures, they suggested a penalization scheme on overhanging surfaces, and an edge analysis was carried out on a benchmark 2D example. The overhang constraint was suggested but not demonstrated.

Wang et al. [36], proposed a novel strategy to reduce the material cost by first extracting the frame structure of the design.

The frame is in fact the solution of a multi-objective optimization problem that minimizes the number of struts while considering stability and printability.

Leary [14] introduced the idea of self-supporting designs, where the TO optimized design was altered to include features similar to support structures. In other words, support structures were introduced as design features *a posteriori*. Since this is carried out after TO, the structural load path is altered, and may violate stress and other performance constraints.

Based on the suggestions proposed by Bracket [12], Gaynor and Guest [16], employed a smooth Heaviside approximation to penalize overhanging surfaces within a SIMP based TO. They demonstrated that, for 2D compliance minimization, this scheme changes the topology to be AM friendly. Specifically, they demonstrated that it is possible to eliminate support structures by suitably changing the TO process. The results are encouraging, but they noted convergence issues when the overhanging penalization was imposed. Recently, Hu et al. [37] proposed a shape optimization technique to alter the model to a more self-supported one. To this end, once a volumetric tetrahedral mesh is generated, the overhang tetrahedra are mapped onto the Gauss sphere and minimally rotated to a self-supported state; the method was also proven to be effective in finding optimal build direction.

3. Proposed method

While we are witnessing significant research activities in TO and AM, a robust framework for integrating the two is lacking. The focus of this paper is to address one aspect of integrating TO and AM, specifically, minimizing support structures.

Consider a typical compliance minimization problem of the form:

$$\begin{aligned} & \text{Minimize } J_{\Omega \subset \Omega_0} \\ & |\Omega| \leq V_f |\Omega_0| \\ & \mathbf{Kd} = \mathbf{f}. \end{aligned} \tag{1}$$

In Eq. (1), $J = \mathbf{f}^T \mathbf{d}$ is the compliance that must be minimized, $|\Omega_0|$ is the initial design volume, Ω is the topology to be computed, and V_f is the desired volume fraction; \mathbf{K} is the stiffness matrix, \mathbf{f} is the external force vector, and \mathbf{d} is the displacement vector.

3.1. The PareTO level-set method

There are several TO methods employed today to solve such TO problems; these include Solid Isotropic Material with Penalization (SIMP) [38–41], level-set [42], [42–44] and evolutionary [45] methods. Among these, we propose to use the level-set based *Pareto Topology Optimization* (PareTO) method [46–48] for the following reasons: (1) in level-set methods, the boundary is well-defined at all times, making it easier to impose support structure constraints, and (2) PareTO relies on the *topological sensitivity* concept (described in Section 3.4) that applies to various performance criteria and constraints, and can be generalized to handle support sensitivity, as discussed in the remainder of the paper.

An important feature of the PareTO method is that it generates Pareto-optimal topologies for various volume fractions. To illustrate, consider the three-hole bracket of Fig. 3, where the two left side holes are fixed and the right hand side hole is subject to a downward unit load. The underlying material is assumed to be isotropic ABS plastic with Young’s modulus of $E = 2$ GPa and Poisson ratio of $\nu = 0.39$.

Fig. 4 illustrates the progression of the optimization process in PareTO up to a volume fraction of 0.5. Observe that optimization begins with a volume fraction of 1.0, and generates multiple

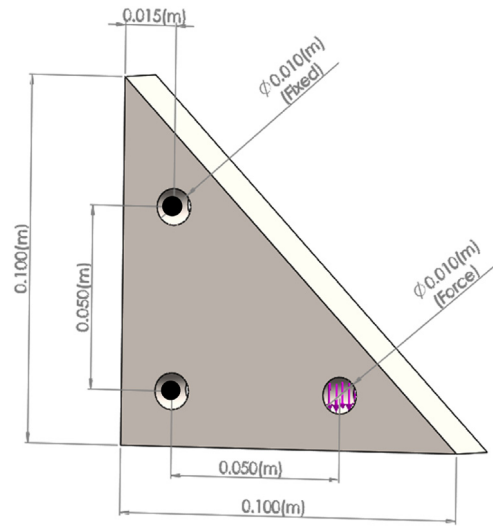


Fig. 3. Three-hole bracket.

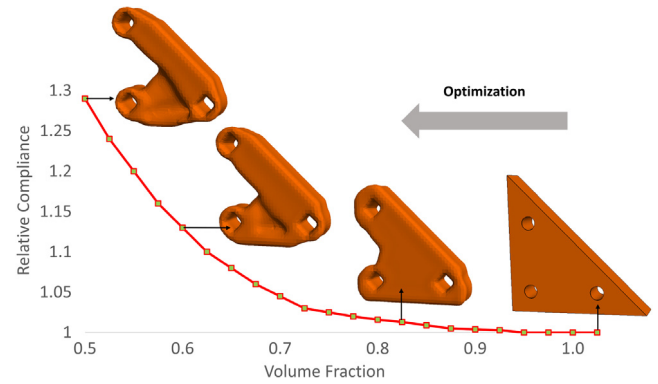


Fig. 4. Pareto curve for three-hole bracket optimization.

topologies that lie on the Pareto curve (Pareto tracing). This will play an important role in the proposed method for constraining the support structure volume. Further, we do not rely on a velocity field concept to move the boundary; instead, we use fixed-point iteration, proposed by [49], to converge to Pareto-optimal designs; the implementation is described in [46–48].

3.2. Limitations of the overhang constraint

Before we discuss how support structure constraints can be imposed, we will briefly review how support structures are algorithmically generated. This will provide key insights into developing appropriate constraints.

Support structure generation in AM is based on the overhang concept which states that *if the angle between the boundary normal and the build direction exceeds a certain threshold, then support structures are needed at that point* [12]. For instance, for the design and the build-direction illustrated in Fig. 5(a), the subtended angle α is illustrated in Fig. 5(b). Given a threshold $\hat{\alpha}$ (typically around 135°), boundary points with $\alpha > \hat{\alpha}$ are considered overhanging, and require support, as illustrated in Fig. 5(c); For simplicity, vertical support structures are assumed in this paper; support structures may terminate at the platform or at any opposing non-overhanging point. The union of all such support structures results in a support volume as illustrated in Fig. 5(d). The fill-ratio, i.e., material density, of support structures is typically less than that of the primary design.

The above definition is exploited both by designers and software algorithms to create suitable support structures; for

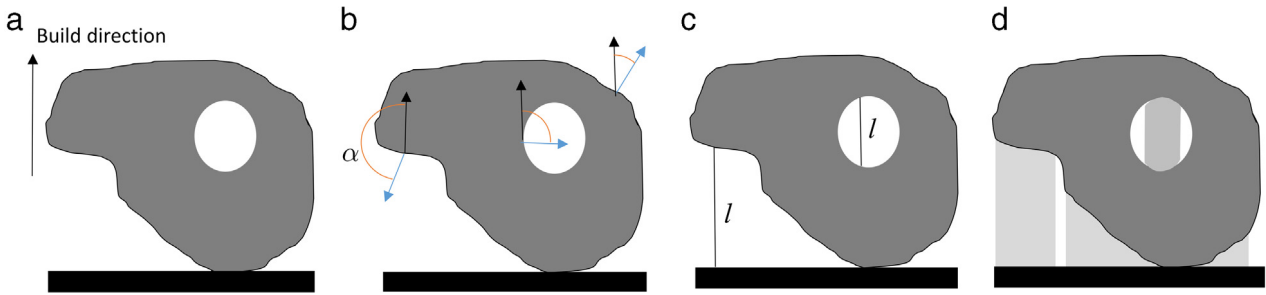


Fig. 5. (a) Build-direction. (b) Subtended angle. (c) Support length. (d) Support volume.

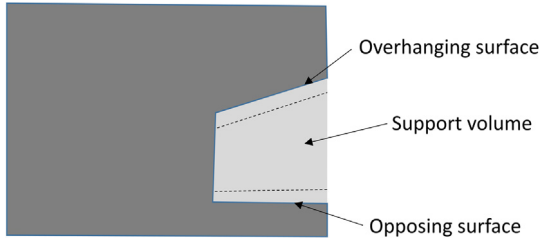


Fig. 6. Moving either the overhanging or its ‘opposing’ surface changes the support volume.

example, see [25]. Further, the definition suggests that if one could eliminate all overhanging surfaces, then support structures can also be eliminated. But, this is not an effective optimization strategy for the following reasons:

1. *Eliminating all overhanging surfaces may not be possible.* Researchers [16] have demonstrated that one can eliminate overhang surfaces in certain 2D problems. However this is unlikely to be successful in general, especially in 3D (as the numerical examples in Section 4 demonstrate). As was also suggested in [6], “...there will probably be instances where it is not necessary for all support structure to be eliminated and so the user should be able to have some control over the strength of the penalty function”.
2. *The overhang constraint does not penalize support volume.* Two overhanging surfaces with equal subtended angle will be penalized equally, although the support volume associated with one may be much larger than the other. To avoid such contradictions, a direct constraint on the support volume is desirable.
3. *Penalizing just the overhanging surfaces is insufficient.* Support volume may be enclosed between an overhanging surface and an opposing surface, as illustrated in Fig. 6. To reduce support volume, both surfaces must be penalized, for example, by moving them closer to each other as illustrated. By penalizing the overhanging surface, only half the problem is addressed.

These limitations suggest that we must seek an alternate, and fundamentally different method to impose constraints on support structures during TO.

We propose here a formulation that relies on (1) dynamically estimating the support volume as the topology evolves, and (2) imposing constraints on the support volume through topological sensitivity methods.

Consider the first step of dynamically estimating the support volume. In this paper, we assume that support structures are vertical. Therefore, the support volume is simply the integral of the support length over the boundary, multiplied by a suitable fill-ratio, (see Fig. 5(d)), i.e.

$$S = \gamma \int_{\alpha \geq \hat{\alpha}} l_p d\Gamma \quad (2)$$

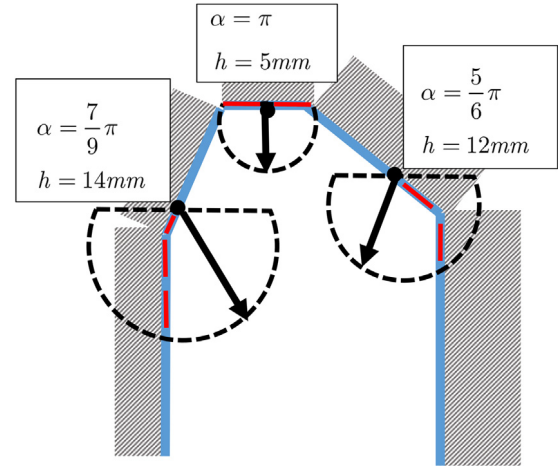


Fig. 7. Searching for self-supporting boundary.

- S : Support structure volume
- α : Subtended angle
- l_p : Length of support structure at boundary point p
- γ : Fill ratio (relative material density) of support structures.

In Eq. (2), the exact value of the fill ratio γ is not critical; it can be assumed to be 0.5, without a loss in generality.

Further, for short overhangs, it is well known that support structures are not needed. For example, for FDM, the allowable overhang [12] can be approximated via:

$$h(\text{mm}) = \begin{cases} 5 + 40(1 - \alpha/\pi); & 3\pi/4 < \alpha \leq \pi \\ \infty & 0 \leq \alpha \leq 3\pi/4. \end{cases} \quad (3)$$

Thus, at any point on the boundary, if the subtended angle is α , support structures are not needed if the overhang distance is less than h given by Eq. (3). In the implementation, we search for self-supporting boundary within a distance given by Eq. (3); see Fig. 7.

3.3. Options for imposing support constraint

Next consider the challenge of imposing support volume constraint. Perhaps the simplest strategy is to impose an absolute constraint as in:

$$S \leq S_{\max}. \quad (4)$$

However, this places an unreasonable burden on the designer to arrive at an absolute value for the upper limit a priori. Instead, we consider relative upper bound constraints. Specifically, recall that in the PareTO method, one generates multiple topologies for various volume fractions, i.e., one can solve the unconstrained problem, and store reference support volumes $S_{unc}(v)$ at intermediate volume fractions v . For example, Fig. 8 illustrates the support volume $S_{unc}(v)$ for the unconstrained problem. The support volume

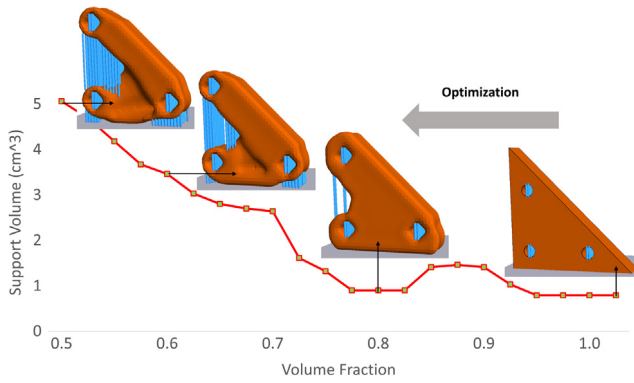


Fig. 8. Relative support structure volume at different volume fractions for unconstrained problem.

curve is, in general, non-smooth, unlike the compliance curve in Fig. 4.

Next we impose a relative constraint with respect to $S_{unc.}(v)$, via a user-defined parameter η ($0 < \eta \leq 1$)

$$S(v) \leq \eta S_{unc.}(v). \quad (5)$$

In other words, Eq. (5) states that the desired support volume should be less than the unconstrained support volume by a factor of η , at each volume fraction (through interpolation, if necessary). Alternately, one can impose a constraint at the final volume fraction, but imposing a constraint at each volume fraction leads to a smoother optimization process. Further, in this paper, we treat Eq. (5) as a ‘soft’ constraint, i.e., the constraint is used to prioritize the solutions within the feasible space (see Section 3.6), rather than limiting this space [50].

In summary, we propose the following support-structure constrained TO problem, where the parameter η ($0 < \eta \leq 1$) is used to strike a balance between performance and AM costs (see numerical experiments in Section 3.8):

$$\begin{aligned} & \text{Minimize } J \\ & \Omega \subset \Omega_0 \\ & |\Omega| \leq V_f |\Omega_0| \\ & S(v) \leq \eta S_{unc}(v) \text{ (soft)} \\ & \mathbf{Kd} = \mathbf{f}. \end{aligned} \quad (6)$$

In Section 3.4, we consider a gradient based TO framework for solving the above problem. The framework will rely on topological sensitivity for performance [51–54], and the proposed topological sensitivity for support structure volume.

3.4. Topological sensitivity of performance

The PareTO method relies on the concept of topological sensitivity for driving the optimization process. To illustrate, consider the structural problem in Fig. 9(a) that represents the design space Ω_0 . Consider now inserting a small *hypothetical* hole that modifies the topology (Fig. 9(b)). Topological sensitivity is the rate of performance change of any quantity of interest φ with respect to the volumetric measure of the hole, i.e., in 2D,

$$\mathcal{T}_\varphi(p) \equiv \lim_{\varepsilon \rightarrow 0} \frac{\varphi(p; \varepsilon) - \varphi}{\pi \varepsilon^2}. \quad (7)$$

If the performance metric is compliance, the field in 2-D is given by the closed-form expression [55]:

$$\mathcal{T}_J(p) = \frac{4}{1+\nu} \sigma : \varepsilon - \frac{1-3\nu}{1-\nu^2} \text{tr}(\sigma) \text{tr}(\varepsilon). \quad (8)$$

Thus the topological sensitivity can be computed as follows: (1) FEA is carried over the domain, (2) stresses and strains

are computed, and (3) then the topological sensitivity field is computed through Eq. (8); the resulting field is illustrated in Fig. 9(c). The interpretation is that regions of low sensitivity correspond to regions with relatively lower impact on performance (and can be removed). Similar topological sensitivity fields can be computed for various performance metrics, both in 2D and 3D [56].

The PareTO method uses the topological sensitivity as a level-set to trace the Pareto curve for decreasing volume fraction. As the topology evolves, the topological sensitivity is recomputed at each iteration. For example, for an intermediate topology in Fig. 10(a), (1) FEA is carried over the new topology, (2) the stresses and strains are computed, and (3) the topological sensitivity field is computed through Eq. (8); the resulting topological sensitivity field is illustrated in Fig. 10(b) and (c).

3.5. Sensitivity of support volume based on surface angle

Analogous to the topological sensitivity for performance, we propose here topological sensitivity of support structure volume, i.e., “the rate of change in support structure volume with respect to volumetric measure of the hole”. Towards this end, consider the two scenarios illustrated in Fig. 11, where the design is infinitesimally perturbed either in the interior, or on the boundary.

Interior hole (Fig. 11(a)): If a hole of radius ε is inserted in the interior of the domain (Ω_ε), one can compute the topological-shape sensitivity as follows. Employing the shape-sensitivity method proposed in [55], the topological derivative is computed via:

$$\mathcal{T}_S(p \in \Omega) \equiv \lim_{\substack{\varepsilon \rightarrow 0 \\ \delta \rightarrow 0}} \frac{S(\Omega_{\varepsilon+\delta}) - S(\Omega_\varepsilon)}{V(B_{\varepsilon+\delta}) - V(B_\varepsilon)}. \quad (9)$$

In Eq. (9), $S(\Omega_\varepsilon)$ and $V(B_\varepsilon)$ are support volume and hole volume, for a hole of radius ε . Using the above definition, one can show that the support volume sensitivity is given by (see Fig. 11(a) and Appendix):

$$\mathcal{T}_S(p \in \Omega) = \frac{3(\pi - \hat{\alpha} - \sin(\hat{\alpha}) \cos(\hat{\alpha})) \left(\sin(\hat{\alpha}) - \frac{\sin^3(\hat{\alpha})}{3} \right)}{\pi} \quad (10)$$

where $\pi/2 \leq \hat{\alpha} \leq \pi$ is the threshold angle. For example, if the threshold angle $\hat{\alpha} = \pi/2$, then $\mathcal{T}_S(p) = 1$, i.e., the entire hole will need to be filled with support structures; a typical value is $\mathcal{T}_S(p \in \Omega) \approx 0.72$ when $\hat{\alpha} = 3\pi/4$.

Boundary hole (Fig. 11(b)): Unlike the interior, the support volume on the boundary depends both on the local neighborhood (curvature) and the length and direction of support. In order to capture both, we define a scalar function $F^S(x_p)$ at each boundary point as follows:

$$F^S(x_p) = \frac{1}{2} l_p (1 - \cos(\alpha_p)). \quad (11)$$

In Eq. (11), α_p is the angle between surface normal and build direction at boundary point p . We compute the sensitivity for the worst-case scenario, where boundary is perturbed along support at each point \hat{s}_p . One can then show the sensitivity at the boundary is given by Eq. (12):

$$\mathcal{T}_S(p \in \partial\Omega) = \frac{1}{2} (1 - \cos(\alpha_p)). \quad (12)$$

Further, for each overhang point, the same sensitivity value is assigned to its corresponding opposite point (see Fig. 6).

Given the above definitions, one can compute the support volume sensitivity at all points; this is illustrated in Fig. 12(b) and (c).

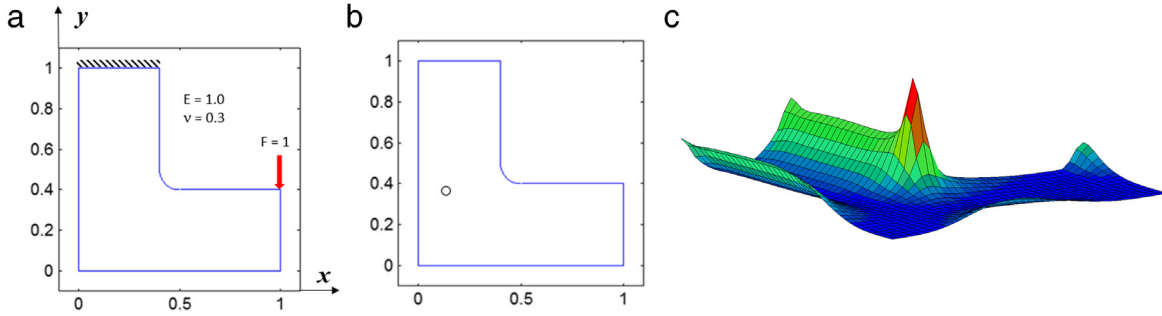


Fig. 9. (a) A structural problem, (b) topological change, and (c) topological sensitivity field.

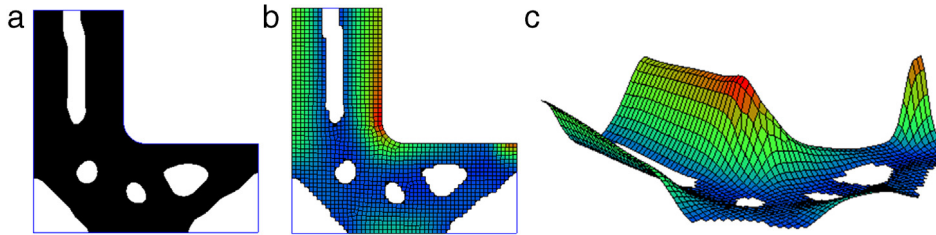


Fig. 10. (a) Instance of topology, (b) compliance topological sensitivity (2D) (c) 3D view of (b).

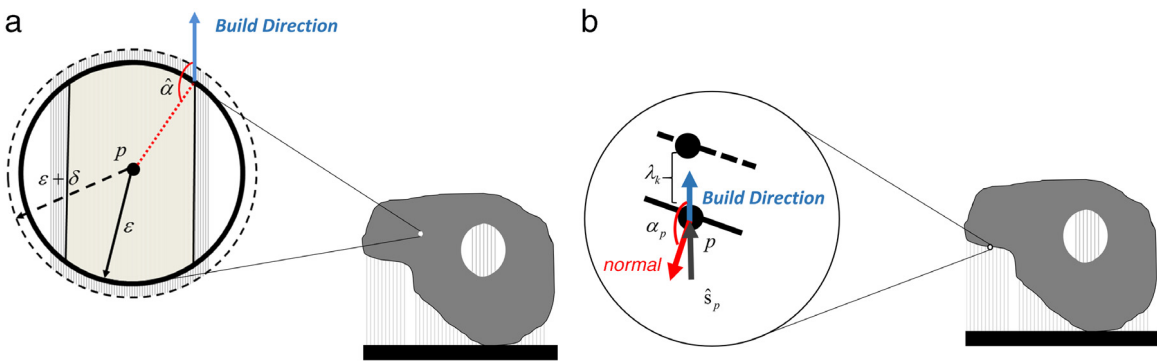


Fig. 11. Sensitivity of support volume, (a) in the interior, (b) on boundary.

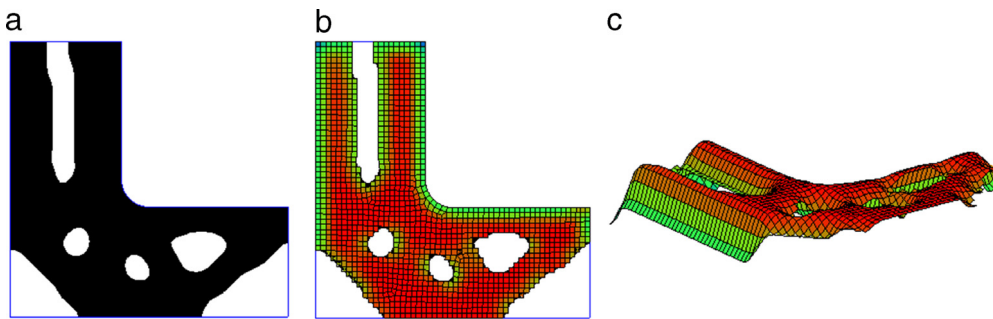


Fig. 12. (a) Instance of topology, (b) Sensitivity of support volume (2D), (c) 3D view of (b).

3.6. Sensitivity weighting

Once the performance and support volume sensitivities are computed and normalized, we exploit the well-established augmented Lagrangian method [57] to impose support structure constraint. Specifically, the support-constrained in Eq. (6) is first expressed in the standard form:

$$g = \frac{S(v)}{\eta S_{unc}(v)} - 1 \leq 0. \tag{13}$$

A popular method for imposing such constraints the augmented Lagrangian method [57], where the constraint and objective are

combined to a single field:

$$\mathcal{L} = J + \mathcal{L}_g$$

$$\mathcal{L}_g = \begin{cases} \mu g + \frac{1}{2} \gamma (g)^2; & \mu + \gamma g > 0 \\ \frac{1}{2} \mu^2 / \gamma & \mu + \gamma g \leq 0 \end{cases} \tag{14}$$

where μ is the Lagrangian multiplier and γ is the penalty parameter (that are updated during the optimization process [57]). By taking the topological derivative of Eq. (14), we arrive at Eq. (15)

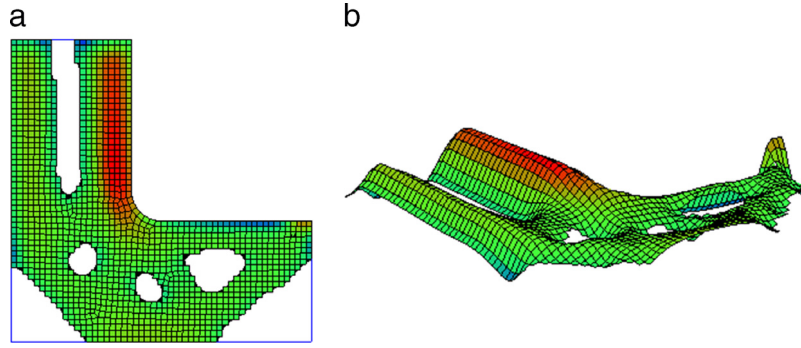


Fig. 13. (a) Equally weighted sum of the two sensitivity fields (2D) (b) 3D view of the sensitivity field.

for the effective sensitivity [58,59]:

$$\mathcal{T} = \mathcal{T}_J + w_S \mathcal{T}_S \quad (15)$$

where

$$w_S = \begin{cases} \mu + \gamma g & \mu + \gamma g > 0 \\ 0 & \mu + \gamma g \leq 0. \end{cases} \quad (16)$$

Observe that the weight on the support structure sensitivity is zero if $g < -\mu/\gamma$, else it takes a positive value. To illustrate Eq. (15), suppose the two topological sensitivity fields are normalized to unity, and suppose $w_S = 1.0$, the resulting field is illustrated in Fig. 13(a) and (b). Observe that the resulting field is a combination of the two fields in Figs. 11 and 12. As the optimization progresses, the weight is determined dynamically from Eq. (15), while the parameters μ and γ are updated during each iteration as described in [58,59]. The algorithm is insensitive to the normalization/scaling of the topological sensitivity fields, i.e., if the fields were not normalized, the computed parameters would be different, but the computed solutions would remain the same. Normalization, however, makes the implementation robust.

3.7. Topological optimization framework

Piecing these concepts together, the proposed algorithm proceeds as follows (see Fig. 14):

1. It is assumed that the unconstrained optimization problem has been solved, and $S_{unc.}(v)$ has been computed.
2. Carry out FEA on Ω ; compute the normalized sensitivity fields $\mathcal{T}_J, \mathcal{T}_S$, and the weighted field \mathcal{T} as described above; smoothen the \mathcal{T} field [47]. Observe that, every time the topology changes, FEA must be executed and the topological sensitivities recomputed.
3. Treating \mathcal{T} as a level-set function, extract a new topology Ω using fixed-point iteration [47], and the iso-surface is extracted [60]. If the topology has not converged, repeat steps 2 and 3.
4. Decrement the volume fraction and return to step 2 until the desired volume is reached.

3.8. Limitations

The proposed sensitivity-based framework assumes a continuous dependence of support volume on boundary/topological perturbation. While this is generally true, the continuity is violated when the overhang angle approaches the critical limit at which the support volume abruptly drops to zero, making it non-differentiable. Due to this discontinuity, the proposed algorithm does not converge to solutions that may be obvious to a human designer. Instead, it converges to other solutions that can be reached in a smooth and continuous manner, as illustrated in the numerical experiments.

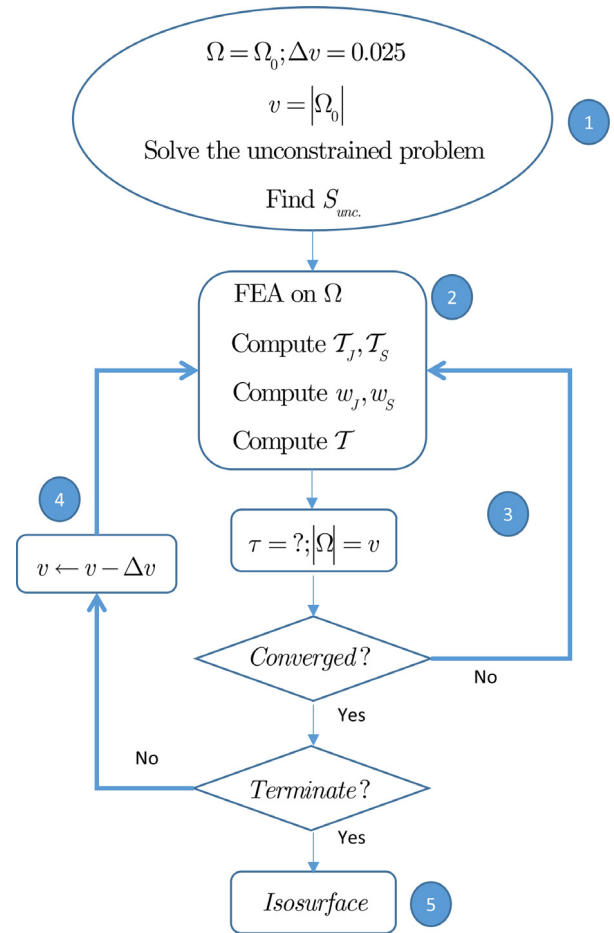







Fig. 14. The proposed algorithm.

4. Numerical experiments

In this section, we demonstrate the proposed method through several examples. In Section 4.1, we study the impact of the proposed method on the optimized design and support volume for a simple 2D example. In Section 4.2, the impact of user controlled parameter η is examined for the three-hole bracket. In Section 4.3, a more complex 3D design is optimized and the designs are printed to demonstrate the effectiveness of the proposed method. In Section 4.4, the effect of build direction on support volume and performance are studied on a large-scale optimization problem. In all of the experiments, the material is assumed to be isotropic ABS plastic with Young's modulus of $E = 2$ GPa and Poisson ratio of $\nu = 0.39$. The threshold angle $\hat{\alpha}$ is assumed to be $3\pi/4$, unless otherwise noted.

Table 1
2D MBB. Effect of support constraint on optimized design.

Final topology	Support volume constraint	Support volume achieved	Relative compliance
	N/A	100%	1.29
	80%	62%	1.34
	60%	59%	1.42
	40%	42%	1.56
	0%	0%	1.75

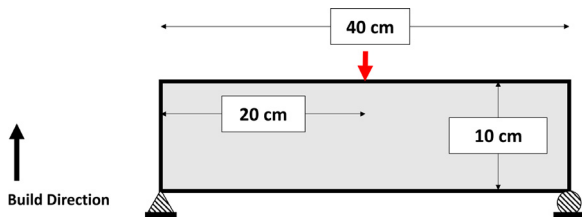


Fig. 15. 2D MBB example with boundary conditions and build direction.

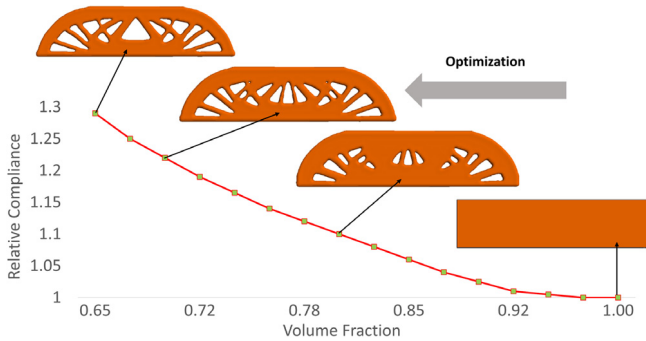


Fig. 16. Compliance Pareto curve for the MBB beam.

4.1. 2D MBB

Consider the 2D MBB design (implicit thickness of 1 cm) in Fig. 15 whose support structure reduction was studied by Gaynor and Guest [16]. The initial design requires no support and the objective is to find stiffest design at 0.65 volume fraction.

Recall that we first solve the unconstrained problem, and a series of topologies that lie on the Pareto curve are generated; see Fig. 16.

Fig. 17 illustrates the corresponding support volume in cm³.

The unconstrained support volume from Fig. 17 is then used as a reference to impose a support structure constraint. In particular, we study the impact of the relative constraint η (see Eq. (6)) on the final topology at a volume fraction of 0.65. Table 1 summarizes the results; observe that with increased support structure constraint, the proposed method reduces the number of internal holes. This

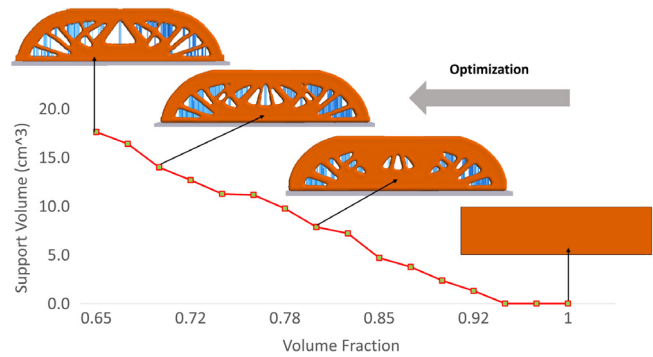


Fig. 17. Support volume for the unconstrained MBB beam problem.

is, by no means, the unique solution to the problem; it happens to be a solution that meets the desired constraints. It remains to be seen if one can generate topologies that meet the support structure constraint and exhibit a better performance.

4.2. Three-hole bracket

In this example, we study the impact of the support structure constraint over the entire Pareto curve. In particular, consider the three-hole bracket illustrated earlier in Fig. 3. Recall the compliance Pareto curve for the unconstrained problem in Fig. 4, and the corresponding support structure curve in Fig. 8. Fig. 18 illustrates the Pareto curves for the unconstrained and the constrained case. As expected, imposing the support constraint increases compliance.

Fig. 19 illustrates the evolution of support structure volume for the two scenarios. Observe that as expected, removing more material can either increase or decrease the support volume due to its nonlinearity, nonetheless imposing a stringent constraint on support structure consistently reduces the support volume w.r.t. the corresponding unconstrained design.

The support volume prior to optimization is $S_0 = 0.79$ (cm³). The objective is to find stiffest design at 0.5 volume fraction. Fig. 20 illustrates the optimized design for (a) unconstrained, (b) constrained with $\eta = 0.50$. Relative compliance values for these cases are respectively 1.29 and 1.58.

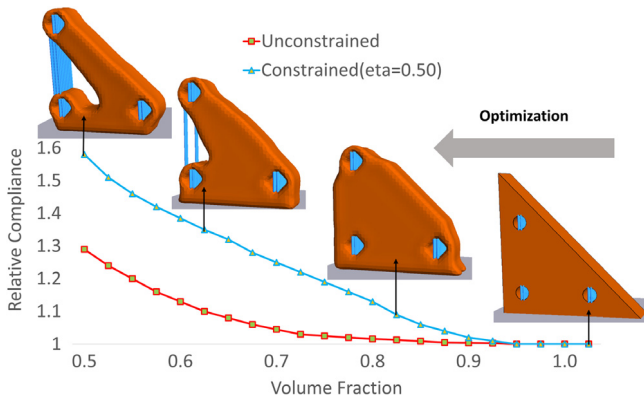


Fig. 18. Unconstrained and constrained Pareto curves for three-hole bracket optimization.

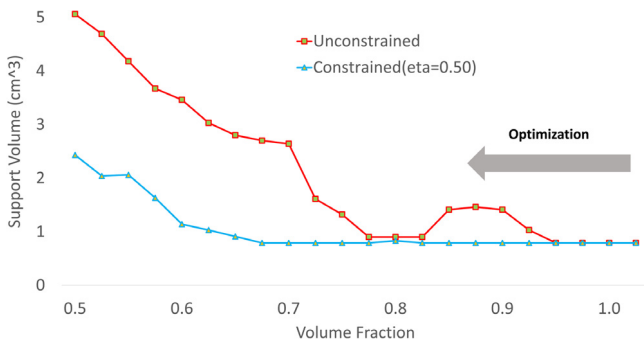


Fig. 19. Evolution of support volume for three-hole bracket.

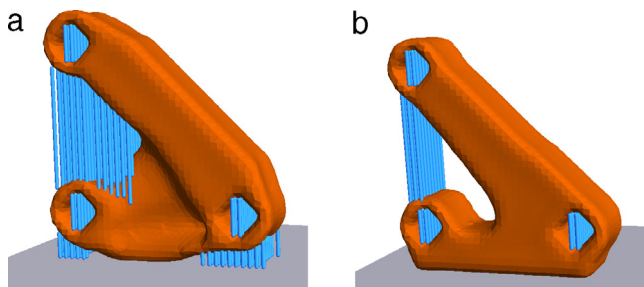


Fig. 20. Optimized three-hole bracket. (a) Unconstrained (b) Constrained with $\eta = 0.50$.

4.3. Mount bracket

Consider the mount bracket of Fig. 21 subject to structural constraints and loading as illustrated. The threshold angle $\hat{\alpha}$ is assumed to be $3\pi/4$. The build direction is illustrated in Fig. 21 since it gives the best surface quality on the larger cylindrical face; for this design, prior to optimization the support volume is $S_0 = 1.12$ (cm^3). The objective is to find stiffest design at 0.7 volume fraction.

Fig. 22 illustrates the optimized designs of (a) unconstrained and (b) constrained with $\eta = 0.80$. The final support structure volume for the unconstrained design is 9.24 (cm^3) while for the constrained design it has reduced by about 17% to 7.70 (cm^3).

Fig. 23 illustrates the evolution of support volume throughout the optimization process. Observe that up to 0.9 volume fraction the unconstrained and constrained results are very similar. However for lower volume fractions the constrained support volume is consistently about 20% smaller than that of unconstrained design.

Fig. 24 illustrates the evolution of relative compliance values as more material is removed from the design. For the unconstrained

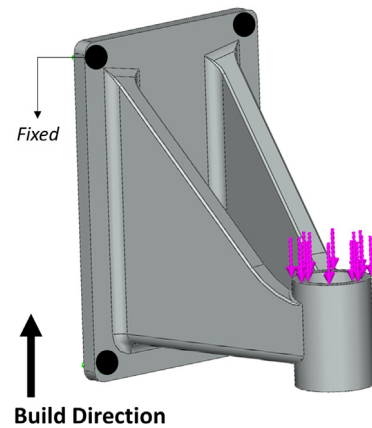


Fig. 21. Mount bracket with boundary conditions and build direction.

design the final (C/C_0) is about 1.05, while by imposing support constraint this value increases to about 2.52. Fig. 24 highlights the trade-off between support volume and compliance when the support constraint is imposed. It is essentially up to the designer to choose the intensity of support constraint.

To verify the validity of these simulated results, each of these topologies were 'printed' on an XYZ Da Vinci 2.0 fused deposition printer. Note that the support structures were not generated by our algorithm, they were introduced by the XYZ software, based on default settings. Fig. 25 illustrates the actual parts after clean-up. Observe that both of the optimized designs have the same weight (as prescribed by the optimization), while the amount of support structure is substantially reduced in the constrained design. This example illustrates the effectiveness of the proposed algorithm in handling support constraints.

4.4. Different build directions

In this section, we demonstrate the robustness of the proposed method with respect to the build directions. Consider the problem posed in Fig. 26 where the geometry is described via numerous curved surfaces and two cylindrical holes in two different directions; this makes picking the optimal build orientation challenging. Further to capture the complexity of the design, a hexahedral mesh with about 1.7 million degrees of freedom was used.

A plausible choice for the build direction is $-Z$, as shown in Fig. 27. In this direction, the larger cylinder has better surface quality and the initial support is minimal. First, we optimize the design for minimum compliance at 0.7 volume fraction without imposing any constraints on support structure.

In this particular orientation, $S_{unc}(0.7)$ is smaller than S_0 , which means that during optimization, some of the overhanging surfaces are removed to reduce the overall support volume. Next, in order to further reduce support structure, we set $\eta = 0.90$ and solved the optimization problem of Eq. (6) to arrive at the design in Fig. 27(b). Observe that by imposing the support constraint, no additional overhangs are created, however since the initial design is dominant, support volume is reduced by only about 3%, while the compliance has increased by about 15%.

Next, the build direction was set to $+Y$ since it gives better surface quality for the smaller cylindrical hole. Solving the same optimization problem as before results in the unconstrained design in Fig. 28(a) and constrained design in Fig. 28(b) with $\eta = 0.90$. The support volume was reduced by 20%, while the compliance increased by 32%.

Finally, the build direction was set to $+X$; a justification for this direction can be better fusion between layers, since the print area

Table 2
Computational cost, with and without support structure constraints.

Example	Finite element degrees of freedom	CPU time unconstrained	CPU time support constrained
MBB	27,400	5.25 s	5.5 s
Three-hole bracket	45,012	10 s	($\eta = 0.75$) 11 s ($\eta = 0.50$) 13.7 s
Mount bracket	196,965	1 min 18 s	1 min 29 s
Rocker Arm (-Z)	~1.7 million	28 min 30 s	30 min 59 s
Rocker Arm (+Y)	~1.7 million	28 min 30 s	32 min 6 s
Rocker Arm (+X)	~1.7 million	28 min 30 s	30 min 14 s

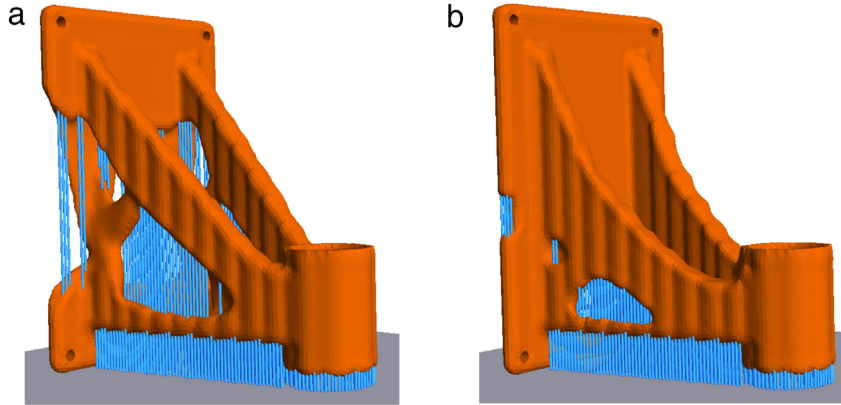


Fig. 22. Optimized mount bracket at 0.7 volume fraction. (a) Unconstrained (b) $\eta = 0.80$.

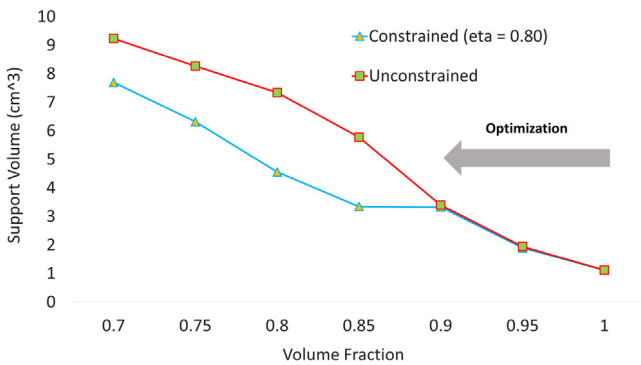


Fig. 23. Evolution of support volume for the mount bracket.

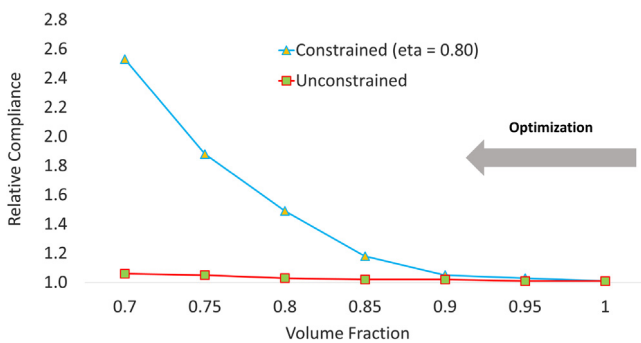


Fig. 24. Evolution of compliance for the mount bracket.

is smaller than previous directions. The results are summarized in Fig. 29: the support volume was reduced by 4%, while the compliance increased by 10%.

4.5. Computational cost

In this section, we study the convergence and performance of the proposed algorithm.



Fig. 25. Printed mount bracket and the required support structures at 0.7 volume fraction.

All experiments are conducted on a Windows 7 64 bit machine with an 8-core Intel Core i7 CPU running at 3.00 GHz, and 16 GB of memory. Table 2 summarizes the CPU times of the unconstrained and constrained examples presented in Sections 4.1–4.3. Observe that as the size of the problem and the support volume increases, the constrained problem requires more computational effort to compute support sensitivity field, yet for all of the presented experiments CPU time remains comparable.

5. Summary and future work

The main contribution of this paper is to propose a topology optimization framework that leads to designs with reduced support structures. Specifically, we introduced a novel topological sensitivity approach for constraining support structure volume during design optimization. The effectiveness of the proposed scheme was illustrated through several numerical examples, and demonstrated using FDM technology.

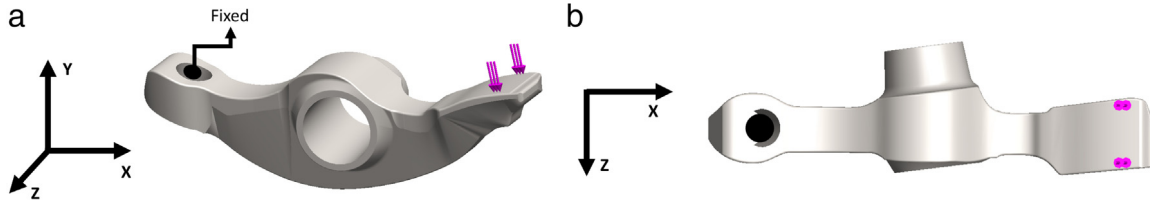


Fig. 26. Rocker arm of Honda Supra-X 100 cc (grabcad.com): (a) Iso view, (b) Top view.

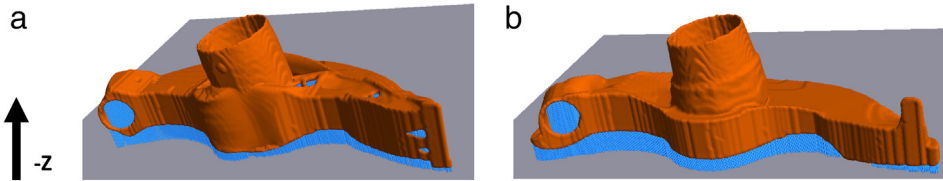


Fig. 27. Rocker arm. Building in $-Z$ direction (a) unconstrained (b) constrained.

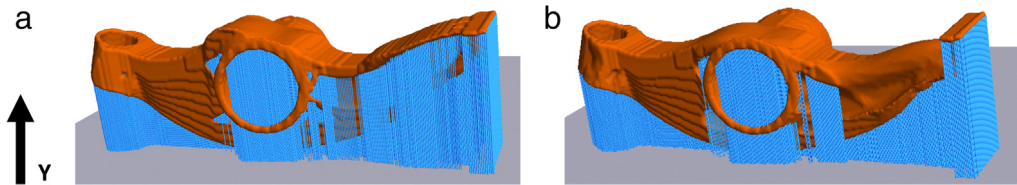


Fig. 28. Build direction along $+Y$ direction: (a) unconstrained, and (b) constrained.

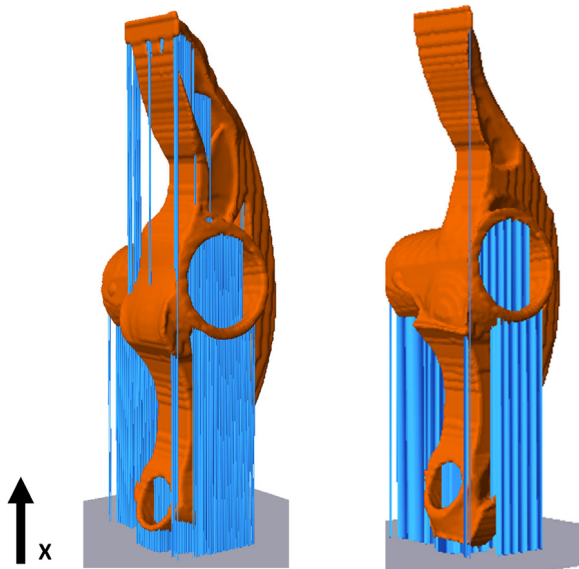


Fig. 29. Rocker arm. Building in $+X$ direction, unconstrained (left) and constrained (right).

Support structures were assumed to be vertical for simplicity, but we believe that the methodology can be extended to handle non-vertical support structures. Additionally, the weighting proposed in this paper is simple and easy to implement. Since there are no benchmark examples in the literature for support volumes, it is difficult to evaluate efficacy of the proposed method.

Finally, the work presented is seen as a first step towards a more comprehensive framework for integrating topology optimization and additive manufacturing. Additional research is needed to include other AM-related constraints, such as surface roughness, volumetric error, inter-layer fusion, and so on. Finally, the proposed method must be coupled with methods for finding the optimum build direction to further reduce support volume.

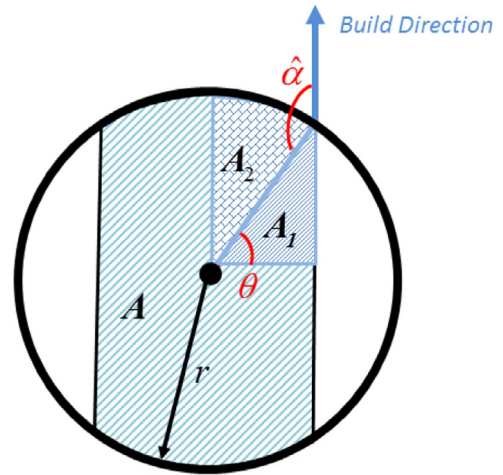


Fig. 30. Support area in a 2D interior hole.

Acknowledgments

The authors would like to thank the support of National Science Foundation through grants CMMI-1561899 and IIP-1500205.

Appendix

In this Appendix, we elaborate on the derivation of Eq. (10). Consider the hole inserted in the interior of the design, we need to find support volume $A = 4(A_1 + A_2)$ (see Fig. 30).

Since $\theta = \hat{\alpha} - \pi/2$ we have:

$$\begin{aligned}
 A_1 &= \frac{1}{2}(r \cos(\theta))(r \sin(\theta)) \\
 &= \frac{1}{2}r^2 \sin(\theta) \cos(\theta) = \frac{-1}{2}r^2 \sin(\hat{\alpha}) \cos(\hat{\alpha}) \quad (17)
 \end{aligned}$$

$$A_2 = \left(\frac{\pi/2 - \theta}{2\pi}\right) \pi r^2 = \frac{(\pi - \hat{\alpha})r^2}{2} \quad (18)$$

$$\mathcal{T}_S(p \in \Omega) = \lim_{\substack{\varepsilon \rightarrow 0 \\ \delta \rightarrow 0}} \frac{4r^3(\pi - \hat{\alpha} - \sin(\hat{\alpha}) \cos(\hat{\alpha})) \left(\sin(\hat{\alpha}) - \frac{\sin^3(\hat{\alpha})}{3} \right) ((\varepsilon + \delta)^3 - \varepsilon^3)}{\frac{4}{3}\pi((\varepsilon + \delta)^3 - \varepsilon^3)} \quad (21)$$

Box I.

$$A = 2r^2(\pi - \hat{\alpha} - \sin(\hat{\alpha}) \cos(\hat{\alpha})). \quad (19)$$

Next to find the support volume in a spherical ball with radius r we extend Eq. (19) as follows:

$$S = \int_{-r \cos(\theta)}^{r \cos(\theta)} 2(r^2 - x^2)(\pi - \hat{\alpha} - \sin(\hat{\alpha}) \cos(\hat{\alpha})) dx$$

$$= 4r^3(\pi - \hat{\alpha} - \sin(\hat{\alpha}) \cos(\hat{\alpha})) \left(\sin(\hat{\alpha}) - \frac{\sin^3(\hat{\alpha})}{3} \right). \quad (20)$$

Finally based on Eq. (9) the topological sensitivity is computed via Eq. (21) given in Box I: i.e.

$$\mathcal{T}_S(p \in \Omega) = \frac{3(\pi - \hat{\alpha} - \sin(\hat{\alpha}) \cos(\hat{\alpha})) \left(\sin(\hat{\alpha}) - \frac{\sin^3(\hat{\alpha})}{3} \right)}{\pi}. \quad (22)$$

References

- [1] Eschenauer HA, Olhoff N. Topology optimization of continuum structures: A review. *Appl Mech Rev* 2001;54(4):331–89.
- [2] Rozvany GIN. A critical review of established methods of structural topology optimization. *Struct Multidiscip Optim* 2009;37(3):217–37.
- [3] Bendsoe M, Sigmund O. Topology optimization: theory, methods and application. 2nd ed. Springer; 2003.
- [4] Kesseler E. Multidisciplinary design analysis and multi-objective optimisation applied to aircraft wing. *WSEAS Trans Syst Control Cybernet* 2006;1(2):221–7.
- [5] Alonso JJ. Aircraft design optimization. *Math Comput Simul* 2009;79(6):1948–58.
- [6] Coverstone-Carroll VH. Optimal multi-objective low-thrust spacecraft trajectories. *Comput Methods Appl Mech Engrg* 2000;186:387–402.
- [7] Wang L. Automobile body reinforcement by finite element optimization. *Finite Elem Anal Des* 2004;40(8):879–93.
- [8] Harzheim L, Graf G. A review of optimization of cast parts using topology optimization: II-Topology optimization with manufacturing constraints. *Struct Multidiscip Optim* 2006;31(5):388–99.
- [9] Krishnakumar A, Suresh K. Hinge-Free compliant mechanism design via the Topological Level-Set. *J Mech Des* 2015;137(3).
- [10] Gibson I, Rosen DW, Stucker B. Additive manufacturing technologies. Springer; 2010.
- [11] Lipson H, Kurman M. Fabricated: the new world of 3D printing. John Wiley; 2013.
- [12] Brackett D, Ashcroft I, Hague R. Topology optimization for additive manufacturing. In: 22nd Annual international solid freeform fabrication symposium. 2011, p. 348–62.
- [13] Dede EM, Joshi SN, Zhou F. Topology optimization, additive layer manufacturing, and experimental testing of an air-cooled heat sink. *J Mech Des* 2015.
- [14] Leary M, Merli L, Torti F, Mazur M, Brandt M. Optimal topology for additive manufacture: A method for enabling additive manufacture of support-free optimal structures. *Mater Des* 2014;63:678–90.
- [15] Maute K, Tkachuk A, Wu J, Qi HJ, Ding Z, Dunn ML. Level set topology optimization of printed active composites. *J Mech Des* 2015.
- [16] Gaynor AT, Guest JK. Topology optimization for additive manufacturing: Considering maximum overhang constraint. In: Presented at the 15th AIAA/ISSMO Multidisciplinary Analysis and Optimization Conference, Atlanta, GA. 2014, p. 16–20.
- [17] Thomas DS, Gilbert SW. Costs and cost effectiveness of additive manufacturing: A Literature review and discussion. NIST, 2014.
- [18] Zhao J. Determination of optimal build orientation based on satisfactory degree theory for RPT. In: Proceedings – ninth international conference on computer aided design and computer graphics. 2005. p. 225–30. Art No. 1604640.
- [19] Pandey PM, Thrimurthulu K, Venkata Reddy N. Optimal part deposition orientation in FDM by using a multicriteria genetic algorithm. *Int J Prod Res* 2004;42(19):4069–89.
- [20] Nezhad AS, Barazandeh F, Rahimi AR, Vatani M. Pareto-based optimization of part orientation in stereolithography. *Proc Inst Mech Eng B* 2010;224(10):1591–8.
- [21] Paul R, Anand S. Optimization of layered manufacturing process for reducing form errors with minimal support structures. *J Manuf Syst* 2014.
- [22] Das P, Chandran R, Samant R, Anand S. Optimum part build orientation in additive manufacturing for minimizing part errors and support structures. 2015.
- [23] Zhang X, Le X, Panotopoulou A, Whiting E, Wang CCL. Perceptual models of preference in 3D printing direction. *ACM Trans Graph* 2015;34(6):215:1–215:12.
- [24] Umetani N, Schmidt R. Cross-sectional structural analysis for 3D printing optimization. *SIGGRAPH Asia* 2013;5:1–4.
- [25] Vanek J, Galicia JAG, Benes B. Clever support: Efficient support structure generation for digital fabrication. *Comput Graph Forum* 2014;33(5):117–25.
- [26] Barnett E, Gosselin C. Weak support material techniques for alternative additive manufacturing materials. *Additive Manuf* 2015;8:95–104.
- [27] Dumas J, Hergel J, Lefebvre S. Bridging the gap: Automated steady scaffolding for 3D printing. *ACM Trans Graph* 2014;33(4):98:1–98:10.
- [28] Chen Y, Li K, Qian X. Direct geometry processing for telefabrication Yong Chen, Kang Li and Xiaoping Qian. *J Comput Inf Sci Eng* 2013;13(4).
- [29] Gebhardt A. Additive manufacturing design and strategies. In: *Understanding additive manufacturing*, A. Gebhardt, Ed. Hanser; 2011. p. 103–28.
- [30] Gibson I, Goenka G, Narasimhan R, Bhat N. Design rules for additive manufacture. In: *International Solid Free Form Fabrication Symposium*. 2010.
- [31] Liu L, Wang C, Shamir A, Whiting E. 3D printing oriented design: geometry and optimization. In *SIGGRAPH Asia* 2014 Courses. 2014, p. (Presentation).
- [32] Seepersad CC, Govett T, Kim K, Lundin M, Pinero D. A designer's guide for dimensioning and tolerancing SLS parts. In: *Solid Freeform Fabrication Symposium*, Austin, TX. 2012, p. 921–31.
- [33] Williams CB, Seepersad CC. Design for additive manufacturing curriculum: A problem-and project-based approach. In: *International solid freeform fabrication symposium*. 2012, p. 81–92.
- [34] Zhou M, Fleury R, Shyy Y-K, Thomas H, Brennan J. Progress in topology optimization with manufacturing constraints. 2002.
- [35] Xia Q, Shi T, Wang MY, Liu S. Simultaneous optimization of cast part and parting direction using level set method. *Struct Multidiscip Optim* 2011;44(6):751–9.
- [36] Wang W, Wang TY, Yang Z, Liu L, Tong X, Tong W, Deng J, Chen F, Liu X. Cost-effective printing of 3D objects with skin-frame structures. *ACM Trans Graph* 2013;32(6):1–10.
- [37] Hu K, Jin S, Wang CCL. Support slimming for single material based additive manufacturing. *Comput-Aided Des* 2015;65:1–10.
- [38] Sigmund O. A 99 line topology optimization code written in Matlab. *Struct Multidiscip Optim* 2001;21(2):120–7.
- [39] Rietz A. Sufficiency of a finite exponent in SIMP (power law) methods. *Struct Multidiscip Optim* 2001;21(2):159–63.
- [40] Du J. Topology optimization of continuum structures with respect to simple and multiple eigenfrequencies. In: 6th World Congresses of Structural and Multidisciplinary Optimization, Rio de Janeiro, 2005.
- [41] Zhou M, Rozvany GIN. The COC algorithm, part II: Topological, geometry and generalized shape optimization. *Comput Methods Appl Mech Engrg* 1991;89(1–3):309–36.
- [42] Allaire G, Jouve F. A level-set method for vibration and multiple loads structural optimization. *Struct Des Optim* 2005;194(30–33):3269–90.
- [43] Wang MY, Wang X, Guo D. A level set method for structural topology optimization. *Comput Methods Appl Mech Engrg* 2003;192:227–46.
- [44] Wang X. Structural shape and topology optimization in a level-set-based framework of region representation. *Struct Multidiscip Optim* 2004;27(1–2):1–19.
- [45] Huang X, Xie YM. A new look at ESO and BESO optimization methods. *Struct Multidiscip Optim* 2008;35(1):89–92.
- [46] Suresh K. A 199-line Matlab code for Pareto-optimal tracing in topology optimization. *Struct Multidiscip Optim* 2010;42(5):665–79.
- [47] Suresh K. Efficient generation of large-scale pareto-optimal topologies. *Struct Multidiscip Optim* 2013;47(1):49–61.
- [48] Mirzendehtel AM, Suresh K. A pareto-optimal approach to multimaterial topology optimization. *J Mech Des* 2015;137(10).
- [49] Cea J, Garreau S, Guillaume P, Masmoudi M. The shape and topological optimization connection. *Comput Methods Appl Mech Engrg* 2000;188(4):713–26.
- [50] Jiang Y, Kautz H, Selman B. Solving problems with hard and soft constraints using a stochastic algorithm for MAX-SAT. In: *Proceedings of the 1st International Workshop on Artificial Intelligence and Operations Research*, Timberline, Oregon, 1995.
- [51] Novotny AA. Topological-shape sensitivity method: Theory and applications. *Solid Mech Appl* 2006;137:469–78.
- [52] Sokolowski J, Zochowski A. On topological derivative in shape optimization. *SIAM J Control Optim* 1999;37(4):1251–72.
- [53] Novotny AA, Feijoo RA, Taroco E. Topological sensitivity analysis for three-dimensional linear elasticity problem. *Comput Methods Appl Mech Engrg* 2007;196(41–44):4354–64.
- [54] Turevsky I, Suresh K. Generalization of topological sensitivity and its application to defeaturing. In: *ASME IDETC Conference*, Las Vegas, 2007.

- [55] Feijoo RA, Novotny AA, Taroco E, Padra C. The topological-shape sensitivity method in two-dimensional linear elasticity topology design. In: *Applications of Computational Mechanics in Structures and Fluids*, CIMNE, 2005.
- [56] Suresh K, Takaloozadeh M. Stress-constrained topology optimization: A topological level-set approach. *Struct Multidiscip Optim* 2013;48(2):295–309.
- [57] Nocedal J, Wright S. *Numerical optimization*. Springer; 1999.
- [58] Deng S, Suresh K. Multi-constrained 3D topology optimization via augmented topological level-set. *Comput & Structures* 2016;170(1):1–12.
- [59] Deng S, Suresh K. Multi-constrained topology optimization via the topological sensitivity. *Struct Multidiscip Optim* 2015;51(5):987–1001.
- [60] Lorensen WE, Cline HE. *Marching Cubes: a high resolution 3D surface reconstruction algorithm*. *ACM siggraph Comput Graphics* 1987;21(4).